Letter

Quantum-metric-induced quantum Hall conductance inversion and reentrant transition in fractional Chern insulators

Ang-Kun Wu [1], Siddhartha Sarkar,[2] Xiaohan Wan,[2] Kai Sun,[2,*] and Shi-Zeng Lin [3,4,†]

[1]Theoretical Division, T-4, Los Alamos National Laboratory (LANL), Los Alamos, New Mexico 87545, USA
[2]Department of Physics, University of Michigan, Ann Arbor, Michigan 48109, USA
[3]Theoretical Division, T-4 and CNLS, Los Alamos National Laboratory (LANL), Los Alamos, New Mexico 87545, USA
[4]Center for Integrated Nanotechnology, Los Alamos National Laboratory (LANL), Los Alamos, New Mexico 87545, USA

(Received 11 July 2024; accepted 29 August 2024; published 12 September 2024)

The quantum metric of single-particle wave functions in topological flat bands plays a crucial role in determining the stability of fractional Chern insulating (FCI) states. Here, we unravel that the quantum metric causes the many-body Chern number of the FCI states to deviate sharply from the expected value associated with partial filling of the single-particle topological flat band. Furthermore, the variation of the quantum metric in momentum space induces band dispersion through interactions, affecting the stability of the FCI states. This causes a reentrant transition into the Fermi liquid from the FCI phase as the interaction strength increases.

DOI: 10.1103/PhysRevResearch.6.L032063

Introduction. The interplay between strong correlation and topology underpins many emergent phenomena in condensed matter systems. A seminal example of this is the discovery of the fractional quantum Hall effect (FQHE) in electron gases subjected to a strong perpendicular magnetic field, forming Landau levels [1–4]. A key feature of the FQHE is the fractionally quantized Hall conductance, which correlates with the Chern number of the Landau level and the fractional filling [3,5–8]. The recent discovery of the fractional Chern insulator (FCI) under zero magnetic field in twisted $MoTe_2$ moiré superlattice [9–12] and pentalayer graphene [13,14] highlights the profound interplay between strong correlation and topology in band systems. In twisted $MoTe_2$, the FCI appears through the partial filling of a topological flat band, with conductance determined by the single-particle band topology [15,16]. In contrast, the emergence of FCI in pentalayer graphene is unexpected since the stabilization of a Chern band itself necessitates interaction.

The behavior of electrons in quantum materials is governed by the energy dispersion and their wave functions in the Hilbert space. An important characterization of the structure of the wave function is the quantum geometric tensor $\eta_{\mu\nu}(\mathbf{k}) \equiv \langle \partial_\mu u_\mathbf{k} | (1 - |u_\mathbf{k}\rangle\langle u_\mathbf{k}|) | \partial_\nu u_\mathbf{k} \rangle$, where $|u_\mathbf{k}\rangle$ is the periodic part of the Bloch wave function [17]. The real part of $\eta_{\mu\nu}$ is the Fubini-Study quantum metric $g_{\mu\nu} = \mathrm{Re}[\eta_{\mu\nu}]$, and the imaginary part is the Berry curvature $F_{xy} = -2\mathrm{Im}[\eta_{xy}]$, which determines the topology of quantum systems. The role of topology in quantum systems has been well recognized, as demonstrated in the integer/FQHE [1,3,18,19], Chern insulators [20], and more recently topological insulators [21] and semimetals [22]. The quantum metric, which is another important aspect of a quantum system, has attracted considerable attention only very recently. Authors of recent studies have shown that quantum geometry can induce transport phenomena [23–27] and can be crucial for the stability of quantum states [28,29], including FCI [30–37]. The stabilization of FCI hinges on several factors, such as band flatness, uniform Berry curvature distribution across momentum space, and the trace condition, which connects the real and imaginary parts of quantum geometry. Theoretically [15,38–44], the approach to achieve an FCI state starts with a flat Chern band, followed by optimizing the quantum geometry of the single-particle wave function [45–55]. Then partially filling the flat topological band stabilizes the FCI with Hall conductance $\sigma_{xy} = C\nu e^2/h$, where C is the Chern number of the band and ν is the filling factor. However, the discovery of FCI in pentalayer graphene challenges this paradigm and calls for a scrutiny of the relationship between the single-particle band and the many-body quantum state.

In this letter, we present an example where the many-body Chern number or Hall conductance deviates from the expected $\sigma_{xy} = C\nu e^2/h$ due to the quantum metric. We examine a model system featuring two distinct single-particle topological bands with $C = \pm 1$. Under strong Coulomb interaction, electrons preferentially populate the band with a lower quantum metric, despite its higher energy at the single-particle level. Consequently, the many-body Chern number diverges from that predicted by the filling of the lower-energy single-particle band. This demonstrates the important role of the quantum metric in FCI phenomena: It not only determines the emergence of the FCI states but also affects the resulting many-body Chern number. Furthermore, the quantum metric generates dispersion through interaction and causes reentrant

*Contact author: sunkai@umich.edu
†Contact author: szl@lanl.gov

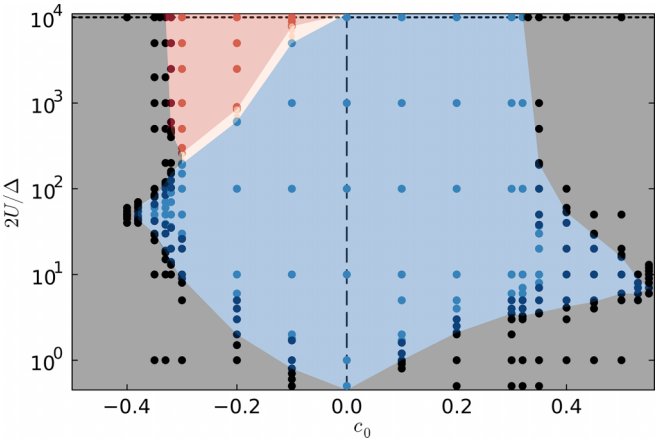

FIG. 1. Phase diagram of the interacting quadratic band crossing point (QBCP) flat bands at $\tilde{\alpha} = 2.13$ with fixed $m_z = 1$ (band gap $\Delta = 2m_z$). The symbols are the calculations with $N_x = 3, N_y = 5$. The red area denotes the fractional Chern insulating (FCI) with inverted many-body Chern number, which originated mainly from the states of the higher single-particle band, while the blue area represents the ordinary FCI mainly contributed from the states in the lower single-particle band. The white area is the crossover region with mixed FCI states from the two bands. Black area represents the Fermi liquid (FL) phase. Vertical dashed line marks the $c_0 = 0$ chiral limit, while horizontal dotted line marks $U \to \infty$ limit. Dark (light) red and blue mark the FCI states with the spread in the FCI ground-state energies larger (smaller) than the many-body gap, indicating more (less) stable FCI states.

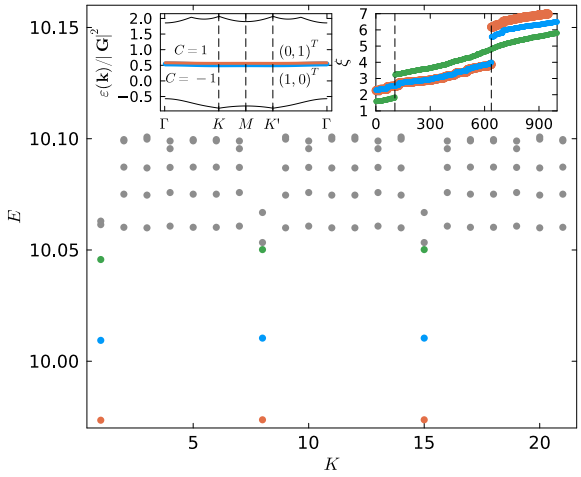

FIG. 2. Many-body state spectrum of the inverted fractional Chern insulating (FCI) at $c_0 = -0.25$, $m_z = 1$ with grid size $N = 21$ (Sec. II in the Supplemental Material [58]) and $Q = 7$ electrons, with infinite U (red region in Fig. 1). Left inset: The single-particle dispersion with the $C = -1$ (blue) band [A sublattice polarized $(1, 0)^T$] lower than the $C = 1$ (red) band [B sublattice polarized $(0, 1)^T$]. Right inset: The particle entanglement spectrum ξ of the three lowest states with a many-body $C_{\rm MB} = \frac{1}{3}$ and the next three lowest states with many-body $C_{\rm MB} = -\frac{1}{3}$ (see Sec. V in the Supplemental Material [58] for the many-body Chern number calculation). Vertical dashed line marks the analytical spectrum gap for the charge density wave (CDW; $N_\xi = 105$) and the FCI ($N_\xi = 637$; Sec. VI in the Supplemental Material [58]).

transition from FCI to Fermi liquid (FL). The multiple roles of the quantum metric give rise to the rich phase diagram, Fig. 1, when tuning the quantum metric through the model parameters and interaction strength.

Model. To establish the connection between the quantum geometry and the many-body quantum state, it is desirable to have great tunability of the quantum geometry and the band dispersion. For this purpose, we take topological flat bands emerging from the quadratic band crossing point (QBCP) with periodic strain [56] as a model system. The physics unraveled here is more general and is applicable to a broad class of systems including twisted bilayer graphene and twisted $MoTe_2$. The QBCP in two dimensions (2D) is described by the continuum Hamiltonian:

$$H_\Gamma(\mathbf{k}) = -\left[c_0 k^2 \sigma_0 - \left(k_x^2 - k_y^2\right)\sigma_x - 2k_x k_y \sigma_y + m_z \sigma_z\right], \quad (1)$$

where σ_α are the Pauli matrices and σ_0 is the identity matrix. All quantities are made dimensionless through proper renormalization. As one lattice realization, the QBCP can emerge as a low-energy theory near the Γ point in a kagome lattice. Adding next-nearest-neighbor hopping in the kagome lattice gives control of the parameter c_0, while an extra phase in the nearest-neighbor hopping gives rise to m_z, which breaks time-reversal symmetry [57]. In the chiral limit $c_0 = 0$ and $m_z = 0$, $\{H_\Gamma(\mathbf{k}), \sigma_z\} = 0$, the spectrum is particle-hole symmetric. To achieve topological flat bands, we introduce periodic strain to the QBCP $H(\mathbf{r}) = H_\Gamma(\mathbf{k}) + A_x(\mathbf{r})\sigma_x + A_y(\mathbf{r})\sigma_y$. In the chiral basis, $k_\alpha \to -i\partial_\alpha$, $z \equiv x + iy$, $\tilde{A} = A_x - iA_y$, $\partial_z = \frac{1}{2}(\partial_x - i\partial_y)$, we have

$$H(\mathbf{r}) = \begin{pmatrix} 4c_0\partial_z\partial_{\bar{z}} - m_z & 4\partial_z^2 + \tilde{A} \\ 4\partial_{\bar{z}}^2 + \tilde{A}^* & 4c_0\partial_z\partial_{\bar{z}} + m_z \end{pmatrix}. \quad (2)$$

Within the first-harmonic approximation [56], the strain field has the form $\tilde{A}(\mathbf{r}) = \frac{\alpha^2}{2}\sum_{n=1}^{3}\omega^{n-1}\cos(\mathbf{G}_n \cdot \mathbf{r} + \phi)$, where α is the strain strength, $\omega = e^{2\pi i/3}$, $\mathbf{G}_1 = \frac{4\pi}{\sqrt{3}}(0, 1)$, $\mathbf{G}_2 = \frac{4\pi}{\sqrt{3}}(-\frac{\sqrt{3}}{2}, -\frac{1}{2})$, $\mathbf{G}_3 = \frac{4\pi}{\sqrt{3}}(\frac{\sqrt{3}}{2}, -\frac{1}{2})$ are reciprocal lattice vectors. In the chiral limit $c_0 = 0$, topological exact flat bands appear at $E = 0$ with Chern number $C = \pm 1$ and ideal quantum metric at specific strain strength $\tilde{\alpha} = \alpha/|\mathbf{G}^m| = 0.79,\ 2.13,\ 3.52, \ldots$. The Chern bands are sublattice polarized, which is defined as the eigenstate of σ_z. The introduction of a finite m_z breaks time-reversal symmetry, raising the energy of one Chern band while lowering the other, with the sign of m_z dictating the sign of the Hall conductance in the noninteracting regime. However, in the regime of strong interaction, especially for the FCI, the quantum metric can reverse the sign of the Hall conductance from that expected in the noninteracting scenario. Beyond the chiral limit, we can adjust the band dispersion and quantum metric of the two low-energy topological flat bands by c_0, deforming the Berry curvature and violating the trace condition [45] (see Sec. I in the Supplemental Material [58]).

To study the interaction effect, we project the density operator onto the two flat bands (red and blue bands in the inset of Fig. 2) and carry out an exact diagonalization (ED)

calculation. The interacting Hamiltonian becomes [15,59,60]

$$H_{\rm int} = \sum_{\mathbf{k},\tau}(\epsilon_{\mathbf{k},\tau} - \mu)c^\dagger_{\mathbf{k},\tau}c_{\mathbf{k},\tau} + \frac{1}{2A}\sum_{\mathbf{q}}\rho(\mathbf{q})V(\mathbf{q})\rho(-\mathbf{q}), \quad (3)$$

where A is the volume (area) of the Brillouin zone (BZ) and $V(\mathbf{q}) = 4\pi U\tanh(qd)/(\sqrt{3}qa)$ is the screened Coulomb potential, where $d = 2a$ is the separation between the electrode and the 2D system, and a is the period of the strain [15]. We label the bands by their Chern numbers $\tau = \pm 1$. The projected density operator is

$$\begin{aligned}\rho(\mathbf{q}) &= \sum_{\mathbf{k},\mathbf{k}',\tau,\tau'}\langle\psi_{\mathbf{k},\tau}|e^{i\mathbf{q}\cdot\mathbf{r}}|\psi_{\mathbf{k}',\tau'}\rangle c^\dagger_{\mathbf{k},\tau}c_{\mathbf{k}+\mathbf{q},\tau'} \\ &= \sum_{\mathbf{k},\tau,\tau'}\lambda_{\tau,\tau',\mathbf{q}}(\mathbf{k})c^\dagger_{\mathbf{k},\tau}c_{\mathbf{k}+\mathbf{q},\tau'}, \quad (4)\end{aligned}$$

where $\psi_{\mathbf{k},\tau}(\mathbf{r}) = e^{i\mathbf{k}\cdot\mathbf{r}}u_{\tau,\mathbf{k}}(\mathbf{r}) = \frac{1}{\sqrt{\Omega}}\sum_{\mathbf{G}}e^{i(\mathbf{G}+\mathbf{k})\cdot\mathbf{r}}u_{\tau,\mathbf{k}}(\mathbf{G})$ is the Bloch state and $\lambda_{\tau,\tau',\mathbf{q}}(\mathbf{k}) = \langle u_{\tau,\mathbf{k}}|u_{\tau',\mathbf{k}+\mathbf{q}}\rangle$ is the form factor. We consider the strong interaction limit where $U \gg W_\tau$, Δ, where W_τ and Δ are the bandwidth and band gap between the $\tau = \pm 1$ bands. When the interband hybridization is neglected, i.e., the single-particle state is sublattice-polarized $\lambda_{\tau,\tau',\mathbf{q}} = \delta_{\tau,\tau'}\lambda_{\tau,\tau,\mathbf{q}}$, the band occupation of electrons is a good quantum number since $[H_{\rm int}, \tau_z] = 0$, where $S^z \equiv \langle\sum_{k,\tau}\tau_z(k,\tau)/2\rangle$ is the band occupation.

In the chiral limit $c_0 = 0$ at the electron filling of $\nu = 1/m$ with m an odd integer, the ground state is FCI due to its ideal trace condition. Here, we focus on $m = 3$, and the conclusion is valid for other values of m. The phase diagram obtained by ED is shown in Fig. 1, where c_0 tunes the quantum metric and the dispersion of the bands. There are two FCI phases (red and blue regions) and the FL phase (gray region). There are two salient features in the phase diagram: (1) In the red regime, the many-body Chern number of the FCI phase is inverted compared with the filling of the lower single-particle band, while in the blue regime, the many-body Chern number aligns with that of the lower single-particle band. (2) When the interaction U increases, there exists a reentrant transition to the FL from the FCI phase around $c_0 = \pm 0.4$. In the following, we show that these two features originated from the quantum metric of the single-particle wave function.

In the chiral limit $c_0 = 0$, there are six degenerate ground states in the ED spectrum, which can be grouped into two sets of FCI states belonging to different band/sublattice polarization. In reality, the system spontaneously selects one band polarization due to symmetry breaking, like spontaneous valley polarization in twisted $MoTe_2$ [10,15] and pentalayer graphene [61]. The FCI nature of the many-body states is confirmed by their total momentum $K = 1, 8, 15$ according to the Haldane rule [62,63] (see Sec. II in the Supplemental Material [58]), and their fractional nature can be confirmed by their many-body Chern number and particle entanglement spectrum gap [42]. From the density distribution $\langle n_{\mathbf{k},\tau}\rangle = \langle c^\dagger_{\mathbf{k},\tau}c_{\mathbf{k},\tau}\rangle$, the six lowest states have a uniform density $\frac{1}{3}$ in each band.

When chiral symmetry is broken ($c_0 \neq 0$), the band occupation is no longer a good quantum number. We consider the weak chiral-symmetry breaking region where the single-particle wave function is still predominantly sublattice polarized and the interband hybridization is small with the help of a sublattice polarization field, $m_z = 1$. In the red region in Fig. 1, the single-particle band with $C = -1$ lies below the band with $C = 1$. Surprisingly, the ground states are the three degenerate FCI states with many-body Chern numbers equal to $C_{\rm MB} = \frac{1}{3}$, which is not expected from the single-particle band. The lowest FCI states have band occupation $S^z \approx Q/2$, which implies that doped electrons occupy the band with $C = 1$, which has a higher single-particle band energy. In the many-body spectrum, the next three lowest degenerate states (blue in Fig. 2) are also FCI states with many-body Chern number $C_{\rm MB} = -\frac{1}{3}$ and have band occupation $S^z \approx -Q/2$. These FCI states correspond to the partial filling of the $C = -1$ lower single-particle band. Interestingly, the third set of three states (green circles in Fig. 2) exhibits a particle entanglement spectrum gap like that of charge density wave (CDW) states, and the density-density correlation peaks in momentum space [47,64]. However, these states never become ground states in the QBCP flat bands when tuning c_0.

Our ED results show that, for a fixed m_z, the many-body Chern number and the sign of the Hall conductance may flip compared with the single-particle band Chern number as the system moves away from the ideal quantum geometry $c_0 = 0$. This inversion of many-body Chern number also occurs for other fractional fillings, i.e., $\nu = \frac{2}{3}, \frac{2}{5}, \frac{2}{7}$ (Sec. IV in the Supplemental Material [58]). To understand this inversion effect, we employ the Hartree-Fock (HF) mean field approximation at integer filling $\nu = 1$ without interband hybridization. The role of the interband hybridization is discussed in Sec. VIII in the Supplemental Material [58]. The self-consistent HF approximation gives

$$E_{\mathbf{k},\tau} = \epsilon_{\mathbf{k},\tau} - \mu + \Delta_H(\mathbf{k},\tau) + \Delta_F(\mathbf{k},\tau), \quad (5)$$

where $\Delta_H(\mathbf{k},\tau)$, $\Delta_F(\mathbf{k},\tau)$ are the Hartree and Fock energies:

$$\begin{aligned}\Delta_H(\mathbf{k},\tau) &= \frac{1}{A}\sum_{\mathbf{q}=n\mathbf{G}}\lambda_{\tau,\mathbf{q}}(\mathbf{k})V(\mathbf{q})\sum_{\mathbf{k}'}\lambda_{\tau',-\mathbf{q}}(\mathbf{k}'), \\ \Delta_F(\mathbf{k},\tau) &= -\frac{1}{A}\sum_{\mathbf{q},\mathbf{k}'=\mathbf{k}+\mathbf{q}}\lambda_{\tau,\mathbf{q}}(\mathbf{k})V(\mathbf{q})\lambda_{\tau,-\mathbf{q}}(\mathbf{k}'). \quad (6)\end{aligned}$$

For a fast decay $V(q)$, we approximate $V(n\mathbf{G}) = V\delta_{n0}$, and $\Delta_H(\mathbf{k},\tau) \approx QV/A$. The Hartree term depends only on density and is independent of the quantum metric of each band.

On the other hand, the Fock contribution can be written as

$$\Delta_F(\mathbf{k},\tau) \approx -\frac{V}{A}\sum_{\mathbf{q},q<q_c}|\lambda_{\tau,\mathbf{q}}(\mathbf{k})|^2 f(E_{\mathbf{k},\tau}), \quad (7)$$

where we have used $\lambda_{\tau,-\mathbf{q}}(\mathbf{k}+\mathbf{q}) = \lambda^*_{\tau,\mathbf{q}}(\mathbf{k})$ and $\tau = \tau'$. It becomes clear that the Fock energy is connected to the Hilbert-Schmidt quantum distance of each band $s^2_\tau(\mathbf{k},\mathbf{k}+\mathbf{q}) \equiv 1 - |\langle u_{\tau,\mathbf{k}}|u_{\tau,\mathbf{k}+\mathbf{q}}\rangle|^2 = 1 - |\lambda_{\tau,\mathbf{q}}(\mathbf{k})|^2$. For a fast decay $V(q)$, we can expand s_τ for small q, $s^2_\tau(\mathbf{k},\mathbf{k}+\mathbf{q}) \approx g_{\tau,\mu\nu}q_\mu q_\nu$. Then the Fock energy becomes

$$\Delta_F(\mathbf{k},\tau) \approx \mathcal{O}(1) + \frac{\pi V_{\rm int}}{A}f(E_{\mathbf{k},\tau}){\rm tr}[g_\tau(\mathbf{k})], \quad (8)$$

with some constant $\mathcal{O}(1)$ and $V_{\rm int} \equiv \int {\rm d}qq^3V(q)$ (see Sec. VII in the Supplemental Material [58]). Thus, the Fock energy depends on the quantum metric of the bands. In the chiral

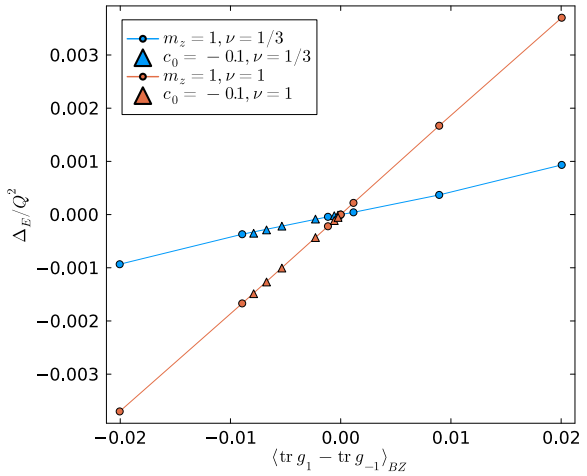

FIG. 3. Energy difference $\Delta_E \equiv \langle E_\tau - E_{-\tau} \rangle_\nu / Q^2$ vs total trace of the quantum metric obtained by exact diagonalization (ED). E_τ is the lowest energy of the states associated with the occupation of the band τ, $\langle \cdots \rangle_\nu$ denotes average over nearly degenerate states, and Q is the total number of electrons at each filling ν with a fixed system size $N = 21$. Circles represent fixed m_z but with varying c_0, while triangles represent fixed c_0 but with varying m_z. The blue curve is for the $\nu = \frac{1}{3}$ fractional Chern insulating (FCI) states (averaged over three nearly degenerate states), while the red curve is for the $\nu = 1$ fully filled Chern insulators.

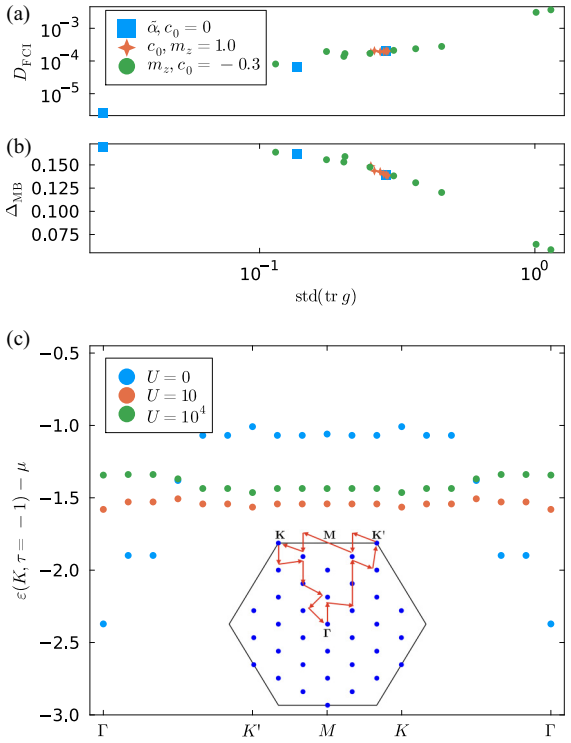

FIG. 4. Quality of fractional Chern insulating (FCI) states vs standard deviation of tr[g] obtained by the exact diagonalization (ED) without interband hybridization. Blue squares are from three different magic parameters $\tilde{\alpha}$ in the chiral limit $c_0 = 0$. Red and green data are obtained at the first magic parameter $\tilde{\alpha}_1 = 0.79$. (a) Spread of the ground state energies for the three quasidegenerate FCI states $D_{\mathrm{FCI}} \equiv E_3 - E_1$. (b) Many-body gap of the FCI states $\Delta_{\mathrm{MB}} \equiv E_4 - E_1$, where E_n denotes nth many-body energy. (c) The lower Hartree-Fock (HF) band dispersion at the cut $c_0 = 0.35$ in Fig. 1, where the reentrant transition to Fermi liquid (FL) occurs. The dispersion is offset by the average band energy $\mu \equiv \langle \epsilon \rangle$, and finite U results are renormalized by U. Here, the system size is $N_x = N_y = 6$.

limit, the trace condition is satisfied $\mathrm{tr}[g(\mathbf{k}, \tau)] = |F_{x,y}(\mathbf{k}, \tau)|$, and $\int d\mathbf{k} |F_{xy}(\mathbf{k}, \tau)| = 1$. The total Fock energy is the same for the $\tau = \pm 1$ band. However, when the chiral symmetry is broken, $\Delta_F(\mathbf{k}, \tau) \propto \mathrm{tr}[g_\tau(\mathbf{k})]$ splits the $\tau = \pm$ bands depending on their quantum metric. The band with a smaller total trace of the quantum metric becomes lower in energy in the strong-interacting limit. Note that $\mathrm{tr}[g_\tau(\mathbf{k})]$ is bounded below by the Berry curvature of the band, so it cannot be zero for a topological flat band.

We verify the above analysis numerically both for $\nu = 1$ and fractional fillings. Indeed, the energy of the occupied band is proportional to the trace of its quantum metric, and the energy difference $\Delta_E \equiv E_{C=1} - E_{C=-1} \propto \sum_{\mathbf{k}} \mathrm{tr}[g(\mathbf{k}, 1) - g(\mathbf{k}, -1)]$, as shown in Fig. 3. One may argue that the HF analysis for a full filling of the band at $\nu = 1$ [Eq. (8)] also applies to FCI because electrons in FCI occupy all momentum points equally. When $c_0 < 0$ and $m_z > 0$, the single-particle band with a higher energy carries a smaller total trace of the quantum metric. As a consequence, the interaction inverts the band energy when it is occupied, which results in an inverted many-body Chern number compared with the expectation of a partial filling of the lower single-particle band.

The first role of the quantum metric in determining the stability of FCI is through the trace condition, i.e., the FCI is favored when $\mathrm{tr}[g(k)] = F_{xy}(k)$. The second role of the quantum metric is to modify the single-particle band alignment and cause the inversion of the many-body Chern number compared with the single-particle band topology. Since the contribution of the quantum metric to the interaction energy is momentum dependent, it also modifies the band dispersion $\Delta_F(\mathbf{k}, \tau) \sim \mathrm{tr}[g_\tau(\mathbf{k})]$, which affects the stability of the FCI. The variation of the quantum metric in the momentum space induces dispersion in the band structure. Here, we introduce the standard deviation of the quantum metric $\mathrm{std}(\mathrm{tr}\, g) \equiv \sqrt{\langle (\mathrm{tr}\, g)^2 \rangle - \langle \mathrm{tr}\, g \rangle^2}$ and study its role in the stability of FCI. We define two quantities to quantify the quality of the FCI states: (a) D_{FCI} is the spread of the otherwise degenerate FCI energy states in the ideal limit; (b) Δ_{MB} is the many-body gap of the FCI state. The smaller the D_{FCI} and the larger the Δ_{MB}, the more robust the FCI. In Fig. 4, the quality of the FCI states is shown to be inversely correlated with the standard deviation of the quantum metric, regardless of the source of deviation ($\tilde{\alpha}$, c_0, or m_z). This is consistent with the expectation that a more dispersive band caused by a large variation of $\mathrm{tr}[g(\mathbf{k})]$ disfavors FCI. As the variation of $\mathrm{tr}[g(\mathbf{k})]$ increases further, the Fock correction to the bands is expected to destroy the FCI states and stabilize the FL [65].

The quantum metric-induced band dispersion also naturally explains the reentrant FL state in the phase diagram, Fig. 1. Around $c_0 = \pm 0.4$, upon increasing U, the system first transits from FL to FCI and then FL. The first transition into FCI is natural since FCI requires interaction dominance

over the kinetic energy of electrons. Our calculations show that the quantum metric also helps flatten the dispersion at intermediate U, as shown in Fig. 4(c). The single-particle band has a strong dispersion around the Γ point, which is compensated by the Fock energy at an intermediate U. For a large U, the HF band becomes dispersive again due to the quantum metric, which induces the second transition from FCI to FL.

In summary, we explore the stability of FCI beyond ideal quantum geometries, particularly for flat bands in systems having QBCP under periodic strain. Using ED and HF calculations, we reveal the significant roles of the quantum metric in stabilizing the FCI. We find that the quantum metric causes the many-body Chern number of the FCI to deviate significantly from the expected value when partially filling the lower-energy single-particle band. Additionally, the variation of the quantum metric in momentum space induces band dispersion through interaction, which impacts the stability of the FCI. As one manifestation, we show the reentrance of FL from the FCI state as the interaction strength increases. Our results have broad implications. For instance, in single-particle band configurations with $C = 0$ and 1, it is possible to have an interaction-induced transition from CDW to FCI if electrons prefer to fill the $C = 0$ or 1 bands depending on the quantum metric. In this letter, we highlight the role of quantum metric in stabilizing the FCI in the strongly correlated topological flat bands and showcase how the resultant FCI deviates from the expectation of partially filling a single-particle band as also exemplified in pentalayer graphene.

Acknowledgments. We thank Heqiu Li, Xi Dai, and Emil Bergholtz for useful discussions. The work at LANL is partially supported by the U.S. Department of Energy (DOE) National Nuclear Security Administration under Contract No. 89233218CNA000001 through the Laboratory Directed Research and Development Program and was performed, in part, at the Center for Integrated Nanotechnologies, an Office of Science User Facility operated for the DOE Office of Science, under user Proposals No. 2018BU0010 and No. 2018BU0083. The work at University of Michigan is partially supported by the Air Force Office of Scientific Research through the Multidisciplinary University Research Initiative, Award No. FA9550-23-1-0334, and the Office of Naval Research Multidisciplinary University Research Initiatives Awards No. N00014- 20-1-2479, No. N00014-21-1-2770, and by the Gordon and Betty Moore Foundation Award No. N031710.

[1] D. C. Tsui, H. L. Stormer, and A. C. Gossard, Two-dimensional magnetotransport in the extreme quantum limit, Phys. Rev. Lett. **48**, 1559 (1982).

[2] H. L. Stormer, Nobel lecture: The fractional quantum Hall effect, Rev. Mod. Phys. **71**, 875 (1999).

[3] R. B. Laughlin, Anomalous quantum Hall effect: An incompressible quantum fluid with fractionally charged excitations, Phys. Rev. Lett. **50**, 1395 (1983).

[4] W. Pan, H. L. Stormer, D. C. Tsui, L. N. Pfeiffer, K. W. Baldwin, and K. W. West, Fractional quantum Hall effect of composite fermions, Phys. Rev. Lett. **90**, 016801 (2003).

[5] N. Trivedi and J. K. Jain, Numerical study of Jastrow-Slater trial states for the fractional quantum Hall effect, Mod. Phys. Lett. B **05**, 503 (1991).

[6] J. K. Jain, Composite-fermion approach for the fractional quantum Hall effect, Phys. Rev. Lett. **63**, 199 (1989).

[7] J. K. Jain, *Composite Fermions* (Cambridge University Press, Cambridge, 2007).

[8] M. Fremling, N. Moran, J. K. Slingerland, and S. H. Simon, Trial wave functions for a composite Fermi liquid on a torus, Phys. Rev. B **97**, 035149 (2018).

[9] H. Park, J. Cai, E. Anderson, Y. Zhang, J. Zhu, X. Liu, C. Wang, W. Holtzmann, C. Hu, Z. Liu *et al.*, Observation of fractionally quantized anomalous Hall effect, Nature (London) **622**, 74 (2023).

[10] J. Cai, E. Anderson, C. Wang, X. Zhang, X. Liu, W. Holtzmann, Y. Zhang, F. Fan, T. Taniguchi, K. Watanabe *et al.*, Signatures of fractional quantum anomalous Hall states in twisted $MoTe_2$, Nature (London) **622**, 63 (2023).

[11] K. Kang, B. Shen, Y. Qiu, Y. Zeng, Z. Xia, K. Watanabe, T. Taniguchi, J. Shan, and K. F. Mak, Evidence of the fractional quantum spin Hall effect in moiré $MoTe_2$, Nature (London) **628**, 522 (2024).

[12] Y. Zeng, Z. Xia, K. Kang, J. Zhu, P. Knüppel, C. Vaswani, K. Watanabe, T. Taniguchi, K. F. Mak, and J. Shan, Thermodynamic evidence of fractional Chern insulator in moiré $MoTe_2$, Nature (London) **622**, 69 (2023).

[13] Z. Lu, T. Han, Y. Yao, A. P. Reddy, J. Yang, J. Seo, K. Watanabe, T. Taniguchi, L. Fu, and L. Ju, Fractional quantum anomalous Hall effect in multilayer graphene, Nature (London) **626**, 759 (2024).

[14] J. Xie, Z. Huo, X. Lu, Z. Feng, Z. Zhang, W. Wang, Q. Yang, K. Watanabe, T. Taniguchi, K. Liu *et al.*, Even- and odd-denominator fractional quantum anomalous Hall effect in graphene moire superlattices, arXiv:2405.16944.

[15] H. Li, U. Kumar, K. Sun, and S.-Z. Lin, Spontaneous fractional Chern insulators in transition metal dichalcogenide moiré superlattices, Phys. Rev. Res. **3**, L032070 (2021).

[16] V. Crépel and L. Fu, Anomalous Hall metal and fractional Chern insulator in twisted transition metal dichalcogenides, Phys. Rev. B **107**, L201109 (2023).

[17] J. Provost and G. Vallee, Riemannian structure on manifolds of quantum states, Commun. Math. Phys. **76**, 289 (1980).

[18] K. v. Klitzing, G. Dorda, and M. Pepper, New method for high-accuracy determination of the fine-structure constant based on quantized Hall resistance, Phys. Rev. Lett. **45**, 494 (1980).

[19] D. J. Thouless, M. Kohmoto, M. P. Nightingale, and M. den Nijs, Quantized Hall conductance in a two-dimensional periodic potential, Phys. Rev. Lett. **49**, 405 (1982).

[20] F. D. M. Haldane, Model for a quantum Hall effect without Landau levels: Condensed-matter realization of the "parity anomaly," Phys. Rev. Lett. **61**, 2015 (1988).

[21] C. L. Kane and E. J. Mele, Z_2 topological order and the quantum spin Hall effect, Phys. Rev. Lett. **95**, 146802 (2005).

[22] X. Wan, A. M. Turner, A. Vishwanath, and S. Y. Savrasov, Topological semimetal and Fermi-arc surface states in the electronic structure of pyrochlore iridates, Phys. Rev. B **83**, 205101 (2011).

[23] C. Wang, Y. Gao, and D. Xiao, Intrinsic nonlinear Hall effect in antiferromagnetic tetragonal CuMnAs, Phys. Rev. Lett. **127**, 277201 (2021).

[24] Y. Gao, S. A. Yang, and Q. Niu, Field induced positional shift of Bloch electrons and its dynamical implications, Phys. Rev. Lett. **112**, 166601 (2014).

[25] D. Kaplan, T. Holder, and B. Yan, Unification of nonlinear anomalous Hall effect and nonreciprocal magnetoresistance in metals by the quantum geometry, Phys. Rev. Lett. **132**, 026301 (2024).

[26] A. Gao, Y.-F. Liu, J.-X. Qiu, B. Ghosh, T. V. Trevisan, Y. Onishi, C. Hu, T. Qian, H.-J. Tien, S.-W. Chen *et al.*, Quantum metric nonlinear Hall effect in a topological antiferromagnetic heterostructure, Science **381**, 181 (2023).

[27] Y. Gao and D. Xiao, Nonreciprocal directional dichroism induced by the quantum metric dipole, Phys. Rev. Lett. **122**, 227402 (2019).

[28] S. Peotta and P. Törmä, Superfluidity in topologically nontrivial flat bands, Nat. Commun. **6**, 8944 (2015).

[29] P. Törmä, S. Peotta, and B. A. Bernevig, Superconductivity, superfluidity and quantum geometry in twisted multilayer systems, Nat. Rev. Phys. **4**, 528 (2022).

[30] S. A. Parameswaran, R. Roy, and S. L. Sondhi, Fractional quantum Hall physics in topological flat bands, C. R. Phys. **14**, 816 (2013).

[31] E. J. Bergholtz and Z. Liu, Topological flat band models and fractional Chern insulators, Int. J. Mod. Phys. B **27**, 1330017 (2013).

[32] T. Neupert, C. Chamon, T. Iadecola, L. H. Santos, and C. Mudry, Fractional (Chern and topological) insulators, Phys. Scr. **T164**, 014005 (2015).

[33] Z. Liu and E. J. Bergholtz, Recent developments in fractional Chern insulators, in *Encyclopedia of Condensed Matter Physics*, 2nd ed., edited by T. Chakraborty (Academic Press, Cambridge, 2024), Vol. 1, p. 515.

[34] N. Morales-Durán, J. Wang, G. R. Schleder, M. Angeli, Z. Zhu, E. Kaxiras, C. Repellin, and J. Cano, Pressure-enhanced fractional Chern insulators along a magic line in moiré transition metal dichalcogenides, Phys. Rev. Res. **5**, L032022 (2023).

[35] N. Morales-Durán, N. Wei, J. Shi, and A. H. MacDonald, Magic angles and fractional Chern insulators in twisted homobilayer transition metal dichalcogenides, Phys. Rev. Lett. **132**, 096602 (2024).

[36] J. Shi, N. Morales-Durán, E. Khalaf, and A. H. MacDonald, Adiabatic approximation and Aharonov-Casher bands in twisted homobilayer transition metal dichalcogenides, Phys. Rev. B **110**, 035130 (2024).

[37] G. Shavit and Y. Oreg, Quantum geometry and stabilization of fractional Chern insulators far from the ideal limit, arXiv:2405.09627.

[38] E. Tang, J.-W. Mei, and X.-G. Wen, High-temperature fractional quantum Hall states, Phys. Rev. Lett. **106**, 236802 (2011).

[39] K. Sun, Z. Gu, H. Katsura, and S. Das Sarma, Nearly flatbands with nontrivial topology, Phys. Rev. Lett. **106**, 236803 (2011).

[40] T. Neupert, L. Santos, C. Chamon, and C. Mudry, Fractional quantum Hall states at zero magnetic field, Phys. Rev. Lett. **106**, 236804 (2011).

[41] D. N. Sheng, Z.-C. Gu, K. Sun, and L. Sheng, Fractional quantum Hall effect in the absence of Landau levels, Nat. Commun. **2**, 389 (2011).

[42] N. Regnault and B. A. Bernevig, Fractional Chern insulator, Phys. Rev. X **1**, 021014 (2011).

[43] J. Dong, J. Wang, P. J. Ledwith, A. Vishwanath, and D. E. Parker, Composite Fermi liquid at zero magnetic field in twisted $MoTe_2$, Phys. Rev. Lett. **131**, 136502 (2023).

[44] B. Hetényi and P. Lévay, Fluctuations, uncertainty relations, and the geometry of quantum state manifolds, Phys. Rev. A **108**, 032218 (2023).

[45] R. Roy, Band geometry of fractional topological insulators, Phys. Rev. B **90**, 165139 (2014).

[46] P. J. Ledwith, G. Tarnopolsky, E. Khalaf, and A. Vishwanath, Fractional Chern insulator states in twisted bilayer graphene: An analytical approach, Phys. Rev. Res. **2**, 023237 (2020).

[47] J. Wang, J. Cano, A. J. Millis, Z. Liu, and B. Yang, Exact Landau level description of geometry and interaction in a flatband, Phys. Rev. Lett. **127**, 246403 (2021).

[48] J. Wang, S. Klevtsov, and Z. Liu, Origin of model fractional Chern insulators in all topological ideal flatbands: Explicit color-entangled wave function and exact density algebra, Phys. Rev. Res. **5**, 023167 (2023).

[49] S. M. Girvin, A. H. MacDonald, and P. M. Platzman, Magneto-roton theory of collective excitations in the fractional quantum Hall effect, Phys. Rev. B **33**, 2481 (1986).

[50] B. A. Bernevig, Z.-D. Song, N. Regnault, and B. Lian, Twisted bilayer graphene. III. Interacting Hamiltonian and exact symmetries, Phys. Rev. B **103**, 205413 (2021).

[51] T. Ozawa and B. Mera, Relations between topology and the quantum metric for Chern insulators, Phys. Rev. B **104**, 045103 (2021).

[52] B. Mera and T. Ozawa, Kähler geometry and Chern insulators: Relations between topology and the quantum metric, Phys. Rev. B **104**, 045104 (2021).

[53] B. Mera and T. Ozawa, Engineering geometrically flat Chern bands with Fubini-Study Kähler structure, Phys. Rev. B **104**, 115160 (2021).

[54] P. J. Ledwith, A. Vishwanath, and D. E. Parker, Vortexability: A unifying criterion for ideal fractional Chern insulators, Phys. Rev. B **108**, 205144 (2023).

[55] M. Fujimoto, D. E. Parker, J. Dong, E. Khalaf, A. Vishwanath, and P. Ledwith, Higher vortexability: Zero field realization of higher Landau levels, arXiv:2403.00856.

[56] X. Wan, S. Sarkar, S.-Z. Lin, and K. Sun, Topological exact flat bands in two-dimensional materials under periodic strain, Phys. Rev. Lett. **130**, 216401.

[57] S. Sarkar, X. Wan, S.-Z. Lin, and K. Sun, Symmetry-based classification of exact flat bands in single and bilayer moiré systems, arXiv:2310.02218.

[58] See Supplemental Material at http://link.aps.org/supplemental/10.1103/PhysRevResearch.6.L032063 for details of momentum discretization, many-body basis and observable calculations.

[59] J. Y. Lee, E. Khalaf, S. Liu, X. Liu, Z. Hao, P. Kim, and A. Vishwanath, Theory of correlated insulating behaviour and spin-triplet superconductivity in twisted double bilayer graphene, Nat. Commun. **10**, 5333 (2019).

[60] Y. Su and S.-Z. Lin, Current-induced reversal of anomalous Hall conductance in twisted bilayer graphene, Phys. Rev. Lett. **125**, 226401 (2020).

[61] T. Han, Z. Lu, G. Scuri, J. Sung, J. Wang, T. Han, K. Watanabe, T. Taniguchi, L. Fu, H. Park *et al.*, Orbital multiferroicity in pentalayer rhombohedral graphene, Nature (London) **623**, 41 (2023).

[62] F. D. M. Haldane, "Fractional statistics" in arbitrary dimensions: A generalization of the Pauli principle, Phys. Rev. Lett. **67**, 937 (1991).

[63] M. D. Johnson and G. S. Canright, Haldane fractional statistics in the fractional quantum Hall effect, Phys. Rev. B **49**, 2947 (1994).

[64] H. Li, Y. Su, Y. B. Kim, H.-Y. Kee, K. Sun, and S.-Z. Lin, Contrasting twisted bilayer graphene and transition metal dichalcogenides for fractional Chern insulators: An emergent gauge picture, Phys. Rev. B **109**, 245131 (2024).

[65] A. Abouelkomsan, K. Yang, and E. J. Bergholtz, Quantum metric induced phases in moiré materials, Phys. Rev. Res. **5**, L012015 (2023).